Quantum waveguide theory: A direct solution to the time-dependent Schrödinger equation

J. B. Wang
Department of Physics, The University of Western Australia, Perth 6907, Australia
and School of Mathematical and Physical Sciences, Murdoch University, Perth 6150, Australia

S. Midgley
Department of Physics, The University of Western Australia, Perth 6907, Australia
(Received 16 November 1998; revised manuscript received 12 March 1999)

In this paper, we present a highly accurate and effective theoretical model to study electron transport and interference in quantum cavities with arbitrarily complex boundaries. Based on this model, a variety of quantum effects can be studied and quantified. In particular, this model provides information on the transient state of the system under study, which is important for analyzing nanometer-scale electronic devices such as high-speed quantum transistors and quantum switches. [S0163-1829(99)02739-3]

I. INTRODUCTION

As electronic circuits get progressingly smaller to the nanometer scale, device analysis based on classical or semiclassical transport theories would eventually fail since the quantum-wave nature of the electrons starts to play a dominant role. Very recent advances in semiconductor fabrication technology have already allowed construction of electronic devices from 500 to 1 nm in size. For example, the DEC21164 microprocessor chip has a circuit pattern with details of size 350 nm.[1] The quantum dots studied at Delft of The Netherlands and at NTT of Japan consist of tunnel barriers of 10 nm thickness.[2] Consequently, electron transport in quantum cavities is receiving great attention worldwide.[3]

A variety of quantum effects have been discovered so far, such as conductance fluctuation, resonant tunnelling, nonlocality, Aharanov-Bohm effect, Kondo resonance, Coulomb blockade, trapped bound states, and nonlinear magnetoconductance.[4–9] These studies raise the possibility of radically new electronic devices with fascinating physics. Several nanodevices have been proposed, e.g., resonant tunnelling diodes, quantum transistors and switches, stub tuners, band filters, and Carbon nanotube quantum resistors (see Refs. 10–13 for an overview). It is expected that further studies will lead to novel quantum devices with outlandish functions that may not yet be foreseen.

Since the characteristic dimensions of nanometer-scale electronic devices are comparable to the wavelengths of electrons with energy from meV to a few eV, theoretical calculations of device properties require a full quantum-mechanical treatment, i.e., by solving the time-dependent Schrödinger equation $i\hbar\partial\psi(\vec{r},t)/\partial t = H\psi(\vec{r},t)$. Current theoretical work on quantum waveguides is predominantly based on the separability of time and spatial variables, which leads to the time-independent Schrödinger equation $H\psi(\vec{r},t) = E\psi(\vec{r},t)$.[14–21]

However, there are severe limitations for the time-independent methods to provide information on transient behavior of the system under study. Much remains to be studied in the temporal response of quantum electronic devices, which is of particular importance for analyzing high-speed quantum transistors and quantum switches. In principle, the general solution of the time-dependent Schrödinger equation can be constructed by a complete expansion of all allowed stationary energy eigenfunctions, but this often requires a very large number of discrete eigen states as well as an integration over the continuous part of the energy spectrum. In terms of accuracy and efficiency, the time-independent methods cannot compete with the time-dependent approach presented in this paper. In addition, the separation of time and spatial variables implies explicitly time-independent Hamiltonian H and thus the electronic transportation properties can only be analyzed under steady-state conditions if the time-independent Schrödinger equation is used.

Another difficulty in solving the time-independent Schrödinger equation lies in the explicit boundary conditions imposed by the various quantum cavities. In some cases, special transformations were carried out to obtain simpler boundaries in the new coordinate system, but this normally gave rise to more complicated differential equations.[19] For this reason, mainly quantum waveguides with very simple geometry have been studied. One can employ the finite element method and the boundary element methods to treat irregular boundaries by dividing the system into scattering and probe regions and then matching the wave functions at the boundaries.[22–26] In this way, the quantum scattering problem is simplified to the solution of a set of algebraic equations. A major difficulty is then the inversion of large matrices, which can be prohibitively expensive in terms of computer memory and CPU time.[23]

In this paper, we employ a highly accurate and effective time-dependent approach to electron transport in quantum cavities. This method was originally developed by quantum chemists to study a variety of gas-phase reactive scattering and related chemical processes in recent years.[27–31] This paper extends their approach to investigate quantum-transport phenomena in condensed matter physics. Undoubtedly, the time-dependent approach has a more natural correspondence to reality, i.e., starting from an initial state of the system and following the events through time. It gives a direct solution of the quantum equations of motion and consequently has many distinct advantages over the traditional time-

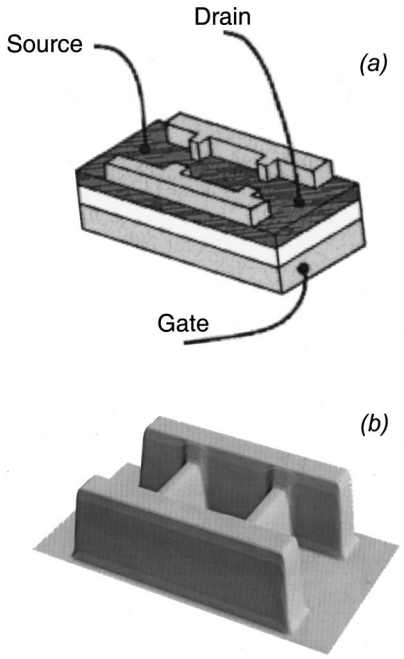

FIG. 1. (a) Schematic diagram of a controlled-barrier atom: gray—metallic, white—insulator, dark—semiconductor; and (b) the external potential imposed on the conduction electrons in the semiconductor.

independent methods. For example, it provides information on transient behaviors and allows direct visualisation of the transport process, where one can ''watch'' a system evolve in real time and as a result monitor intermediate stages of the process of interest. As an initial value problem, it is also comparatively easy to implement, flexible, and versatile in treating a large variety of quantum problems. Another very important attribute of this approach is that it can be applied to study quantum waveguides with arbitrarily complex boundaries and is free of the difficulties encountered by time-independent methods.

The outline of the paper is as follows: In Sec. II, we describe the structure of the nanodevice under study and discuss an effective theoretical scheme for solving the time-dependent Schrödinger's equation. Section III presents computer-simulated results and a stringent verification of their accuracy. Finally, conclusions are drawn in Sec. IV.

II. THEORY

As a prototype case, we examine a simple nanoelectronic device similar to that described by Kastner[32] as a controlled-barrier artificial atom. The device is illustrated schematically in Fig. 1(a), where the gray areas are metallic, white area is insulating ($Al_xGa_{1-x}As$) and dark area is semiconducting (GaAs). When a negative voltage is applied to the two metal stripes on the top surface of the GaAs, the accumulated electrons in the metal stripes form potential walls and barriers due to repulsive Coulomb force, which control the motion of the conduction electrons in the semiconductor (GaAs). Shown in Fig. 1(b) is a typical potential imposed on the conduction electrons. The electron motion is restricted to two dimensions due to the narrow quantum well formed at the $GaAs/Al_xGa_{1-x}As$ interface, which essentially forbids motion perpendicular to the interface. Very recently, Kane *et al.* developed a new quantum-wire fabrication technique that eliminates the need for a dopant layer in the heterostructures adjacent to the two dimensional electrons.[33] Consequently, the quantum cavity is free of the impurity that may be introduced by modulation doping and has essentially perfect crystalline structure.

Quantum cavities in the nanometer scale are frequently referred to as single-electron tunneling devices, since their central channels often hold but a single-conduction electron. Of course there are many other electrons in the semiconductor, because they are fabricated in solids not in vacuum, but almost all of them are tightly bound to the nuclei in the solid. Accordingly, electron-electron correlation effect on electron transportation properties is small. This independent electron approximation of mesoscopic structures is supported by many experiments.[34] Also, at low temperatures of several Kelvin, the energy of phonons is too low to interact with the electrons and can often be neglected.[35] Both the electron mean-free path and the phase coherence length are greater than the sample dimension. If, in addition, the few conduction electrons in the semiconductor stay near the bottom of the conduction band during the tunneling process and the external potential is not strong enough to induce interband transitions, the standard single-electron effective-mass approximation is then valid.

Because of the interaction with the crystal lattice in the nanostructures, the conduction electrons appear to have a different mass from m_e.[36] In this case, the time-dependent Schrodinger equation for describing a two-dimensional electron transport in the potential of the lattice plus the potential of an applied external potential $V(x,y)$ is given as

$$i\hbar\frac{\partial}{\partial t}\psi(x,y,t)=-\frac{\hbar^2}{2m^*}\left(\frac{\partial^2}{\partial x^2}+\frac{\partial^2}{\partial y^2}\right)\psi(x,y,t)+V(x,y)\psi(x,y,t), \tag{1}$$

where $m^*=0.066$ a.u is the effective mass for GaAs (Ref. 37) and the system Hamiltonian is

$$H=-\frac{\hbar^2}{2m^*}\nabla^2+V(x,y)=-\frac{\hbar^2}{2m^*}\left(\frac{\partial^2}{\partial x^2}+\frac{\partial^2}{\partial y^2}\right)+V(x,y). \tag{2}$$

The formal solution of the time-dependent Schrodinger equation with time-independent Hamiltonian is $\psi(x,y,t+\Delta t)=\exp(-iH\Delta t)\psi(x,y,t)$. Although this general solution has been available for quite some time,[38,39] computational techniques for treating the exponential time propagator $\exp(-iH\Delta t)$ had been slow to develop and practical calculations have had to await the arrival of powerful computers. Different approximations to the exponential time propagator $\exp(-iH\Delta t)$ along with the technique used to evaluate the action of the Laplacian ∇^2 on the wave function lead to different time evolution schemes.

The simplest scheme expands the exponential function to the first order, i.e., the Euler expansion $\psi(\mathbf{r},t+\Delta t)=(1-iH\Delta t)\psi(\mathbf{r},t)$. This scheme is not symmetric with respect to time and is therefore unstable. It is also not unitary. To avoid this instability, McCullough and Wyatt[40] used a first-order difference scheme with a unitarised approximation to

the time evolution propagator (FOD), $\psi(\mathbf{r},t+\Delta t)=[(2-iH\Delta t)/(2+iH\Delta t)]\psi(\mathbf{r},t)$. This scheme is unitary and unconditionally stable, but large matrices need to be inverted, which can be prohibitively expensive in terms of computer memory and CPU time. To overcome this problem, Askar and Cakmak[41] developed an explicit second-order differencing scheme (SOD), $\psi(\mathbf{r},t+\Delta t)-\psi(\mathbf{r},t-\Delta t)=-2iH\Delta t\psi(\mathbf{r},t)$. It is unitary, symmetric in time and shown to be conditionally stable.

The drawback of these finite difference type of methods is that the associated truncation error is proportional to $(H\Delta t)^2$. For this reason, the time step Δt for each propagation has to be extremely small and, therefore, the number of steps required for modeling a complete scattering event is very large. Although both FOD and SOD schemes conserve the norm and energy, errors will accumulate in the phase. There are other existing explicit and implicit propagation schemes based on a Taylor expansion of the time evolution operator.[42] However, all these methods require small time steps and thus suffer the same problem of error accumulation, which may cause severe distortion of the wavepackets.

Another propagation scheme worth mentioning is the split operator method (SPO) devised by Feit, Fleck, and Steiger.[43] It splits the exponential operator into three parts and then treats them consecutively in their diagonal representations, i.e.,

$$\psi(\mathbf{r},t+\Delta t)=\exp(-i\Delta t\nabla^2/2)\exp(-i\Delta tV)\times\exp(-i\Delta t\nabla^2/2)\psi(\mathbf{r},t).$$

This method is unconditionally stable and norm-preserving, since only unitary operators are involved. It has been used widely and, in many cases, successfully in wavepacket studies. Nevertheless, this scheme neglects the commutators between the potential and kinetic-energy operators and thus introduces error in both energy and phase in wave functions. The magnitude of the inaccuracy depends strongly on the system under investigation.[44]

A more accurate and stable method is the Chebyshev scheme, pioneered by quantum chemists Tal-Ezer and Kosloff.[27] We applied this scheme to one-dimensional potential scattering and our results were in excellent agreement with exact solutions.[45] This paper extends our previous work to two dimensions to study electron transport in nanoquantum waveguides. Briefly, the Chebyshev scheme approximates the exponential time propagator by a Chebyshev polynomial expansion:

$$\psi(x,y,t)=\exp[-i(E_{\max}+E_{\min})t/2]\times\sum_{n=0}^{N}a_n(\alpha)\phi_n(-i\tilde{H})\psi(x,y,t=0), \quad (3)$$

where $E_{\max}$ and $E_{\min}$ are the upper and lower bounds on the energies sampled by the wavepacket, $\alpha=(E_{\max}-E_{\min})t/2$, $a_n(\alpha)=2J_n(\alpha)$ except for $a_0(\alpha)=J_0(\alpha)$, $J_n(\alpha)$ are the Bessel functions of the first kind, ϕ_n are the Chebyshev polynomials, and the normalized Hamiltonian is defined as

$$\tilde{H}=\frac{1}{E_{\max}-E_{\min}}[2H-(E_{\max}+E_{\min})]. \quad (4)$$

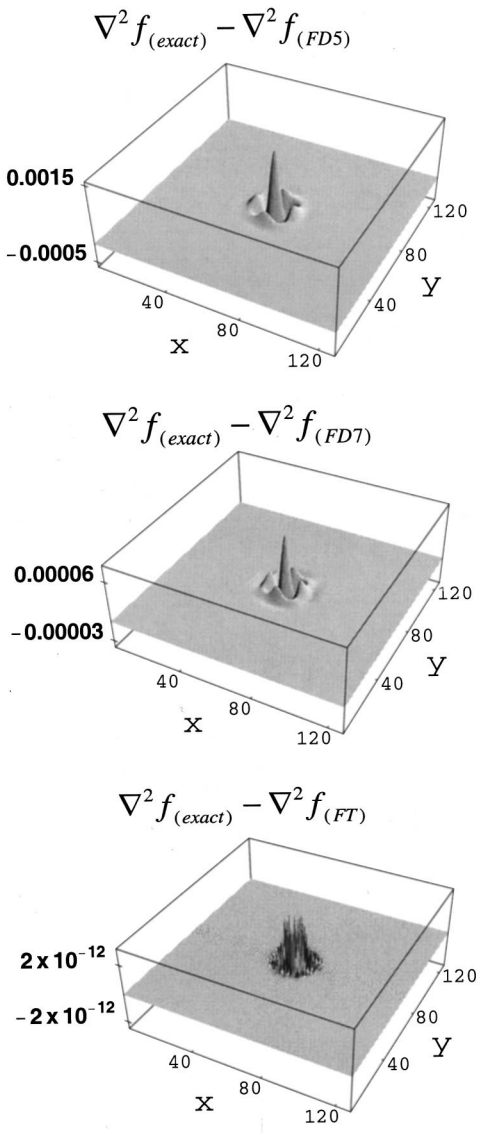

FIG. 2. Absolute errors in evaluating the second derivative of a Gaussian function using (a) the five-point finite-difference method; (b) seven-point finite-difference method; and (c) the Fourier transformation method.

The above normalization ensures that the expansion of Chebyshev polynomials is convergent. Since the Bessel function falls to zero exponentially as n increases beyond α, it follows that terminating the expansion at $N>\alpha$ would yield accurate results. Note, α is proportional to the time step t and so is the number of terms required in the expansion. Since the time step t can be arbitrarily large, this scheme is often used as a one-step propagator to cover the complete interaction.

The action of the operator $\phi_n(-i\tilde{H})$ on the initial wavefunction $\psi(\mathbf{r},0)$ can be evaluated using the following recurrence relation:

$$\phi_{n+1}(-i\tilde{H})\psi(\mathbf{r},0)=-2i\tilde{H}\phi_n(-i\tilde{H})\psi(\mathbf{r},0)+\phi_{n-1}(-i\tilde{H})\psi(\mathbf{r},0) \quad (5)$$

with $\phi_0(-i\tilde{H})\psi(\mathbf{r},0)=\psi(\mathbf{r},0)$ and $\phi_1(-i\tilde{H})\psi(\mathbf{r},0)=-i\tilde{H}\psi(\mathbf{r},0)$. The calculation therefore boils down to a se-

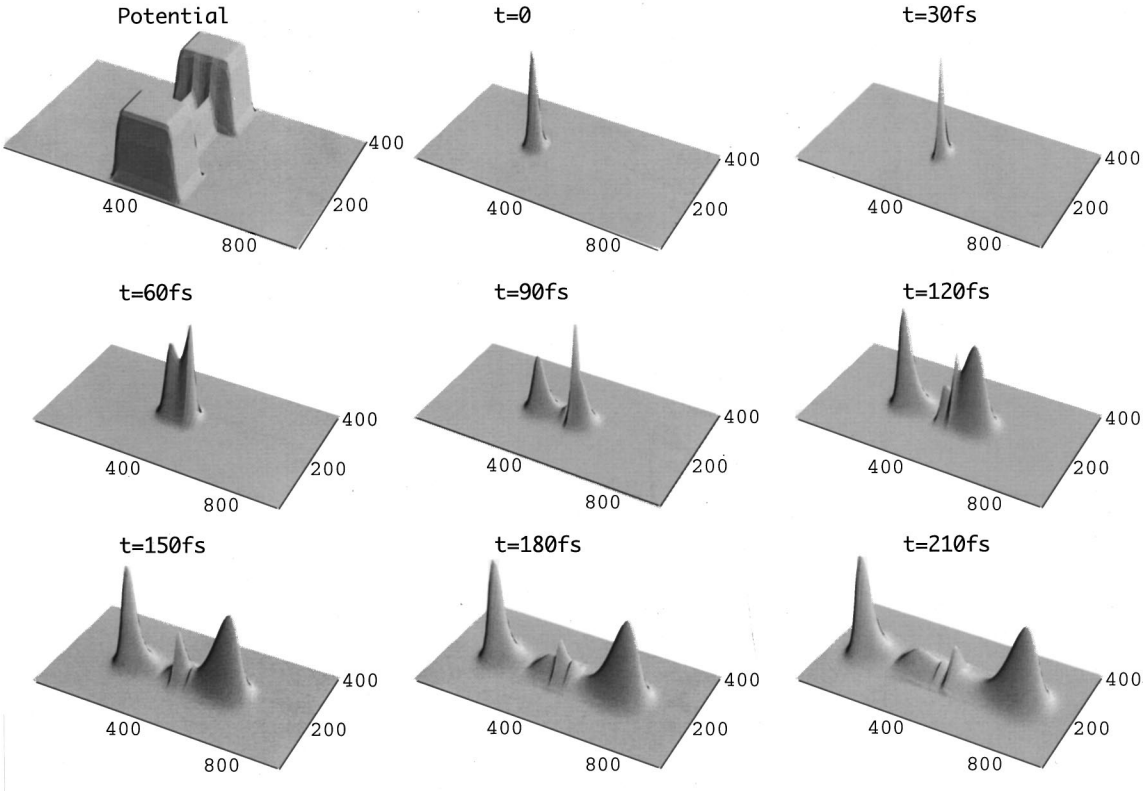

FIG. 3. Time evolution of the system wave function in coordinate space. The grid size is 1000 nm×420 nm. The potential heights of the sidewalls and the barriers are 2 and 0.98 eV, respectively. The initial energy of the electron wave packet is 1 eV.

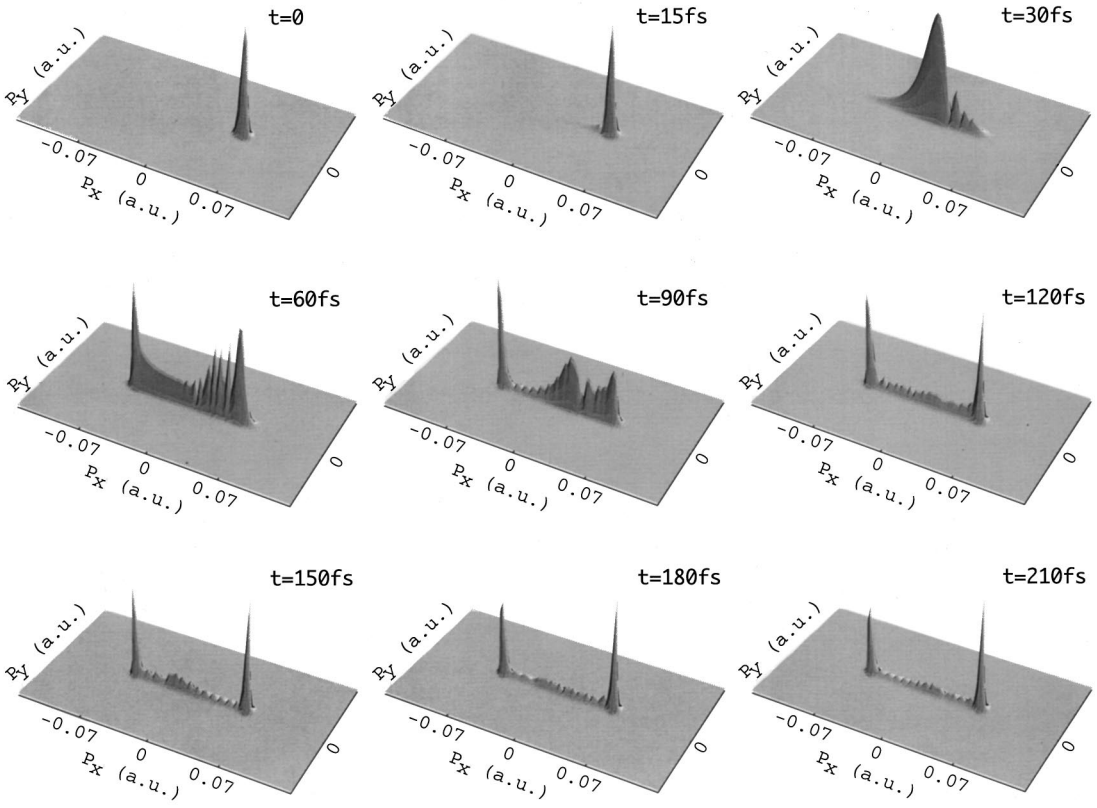

FIG. 4. Time evolution of the system wave function in momentum space for the same potential and initial energy as Fig. 3.

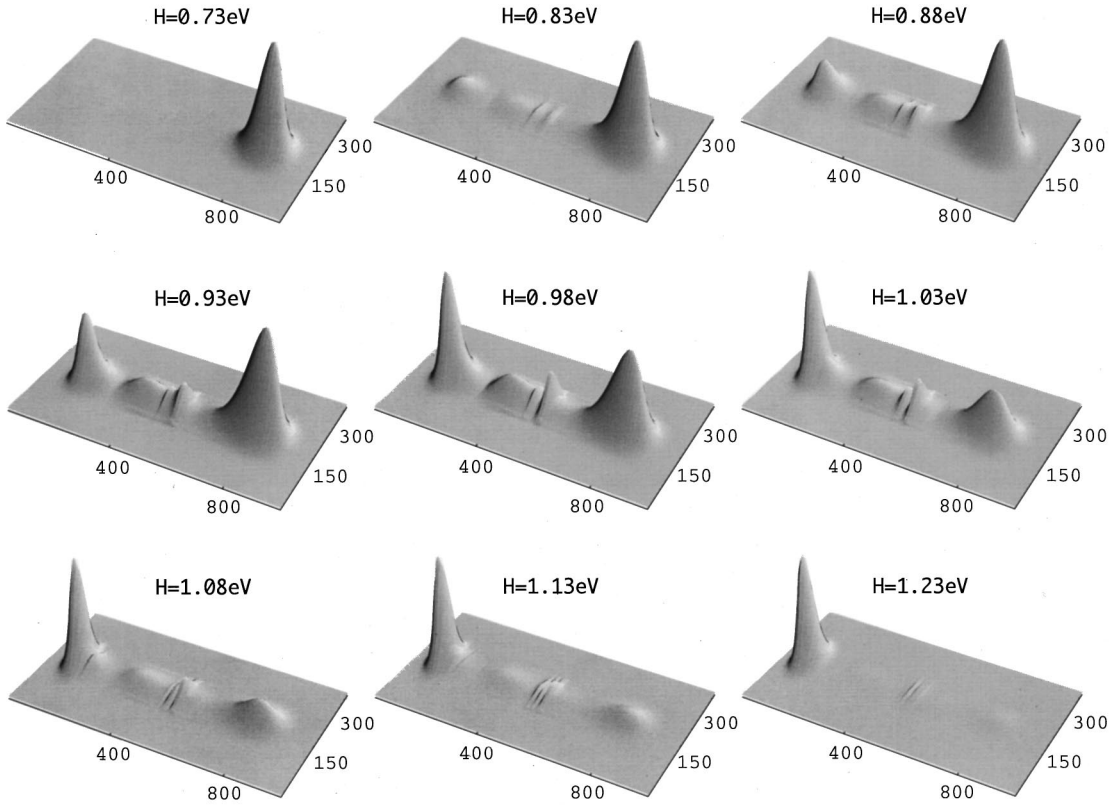

FIG. 5. System wave function at $t=210$ fs for different barrier heights (H). The grid size is 1000 nm$\times$420 nm and the initial energy of the electron wavepacket is 1 eV.

ries of calculation of the Hamiltonian $\tilde{H}$ acting on some function, which can be split into two parts: (i) the straightforward scalar multiplication $V(x,y)f(x,y)$; and (ii) the second-order derivative $\nabla^2 f(x,y)$. An accurate evaluation of the derivatives is a prerequisite for obtaining reliable time-dependent wave functions. In this paper, we adopted the Fourier transformation method (FT), i.e.,[30]

$$\nabla^2 f(x,y)=\int\int [(i2\pi k_x)^2 + (i2\pi k_y)^2]F(k_x,k_y)e^{i2\pi(k_x x+k_y y)}dk_x dk_y, \tag{6}$$

where

$$F(k_x,k_y)=\int\int f(x,y)e^{-i2\pi(k_x x+k_y y)}dxdy. \tag{7}$$

Figure 2 shows the absolute error $\nabla^2 f_{(\text{exact})}-\nabla^2 f_{(\text{numerical})}$ in evaluating the second derivative of a Gaussian function. The numerical error of the FT scheme is found to be nine and seven orders of magnitude smaller than that of the five-point and seven-point finite-difference method, respectively. We also checked the FT scheme for several arbitrarily deformed wave functions. The same accuracy is achieved in evaluating their derivatives as long as the wavefunctions approach zero at the boundaries. It is important to note that, if the fast Fourier transform (FFT) method is used to compute derivatives, care must be taken to ensure that the wave function is effectively zero along the boundaries at all times. This is because the FFT method implies periodic boundary conditions and, as a result, the wave packet crossing one boundary would reemerge on the opposite side giving rise to unwanted artifact.

III. RESULTS AND DISCUSSIONS

In this section, we employ the Chebyshev propagation scheme together with the fast Fourier transformation method to obtain solutions of Eq. (1). The initial wave function $\psi(x,y,t=0)$ is assumed to be a Gaussian of the form

$$\psi(x,y,t=0)=\frac{1}{2ab\pi}\exp\left[-2\left(\frac{x-x_c}{2a}\right)^2 - 2\left(\frac{y-y_c}{2b}\right)^2\right]\exp(ip_x x+ip_y y), \tag{8}$$

where (x_c,y_c) denotes the center of the initial Gaussian wave function, p_x and p_y are respectively the peak value of its momentum in the x and y direction, a and b define the spread of the wave function in coordinate space, which in turn determine its spread in momentum space and vice versa.

For the following calculation, the prototype device is taken as 200 nm in length and 400 nm in width, while the spatial grid is chosen to be 1000 nm long and 420 nm wide to accommodate the wave packet throughout the tunneling. The heights of the two potential walls and the two barriers are, respectively, 2 and 0.98 eV. The initial energy of the electron wave packet is chosen to be 1 eV, corresponding to $p_x=0.07$ a.u. and $p_y=0.0$ a.u. The momentum spread is as-

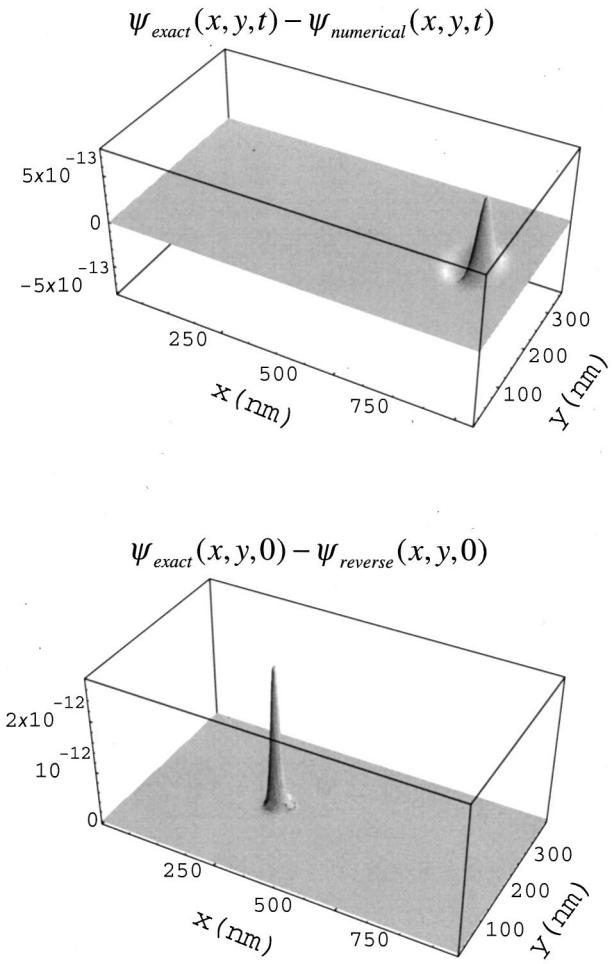

FIG. 6. (a) Absolute error between exact analytical solution and numerical propagation of a Gaussian wave function through free space; (b) absolute error between initial wave function and the wave function propagated forward and then backward in time to $t=0$.

sumed to be 5% in both x and y directions. The center of the initial wavepacket (x_c, y_c) is set sufficiently away from the potential barriers to ensure that the entire wave function has negligible interaction with the potential at time $t=0$.

Figure 3 illustrates the time evolution of the electron wave packet provided by Eq. (3), together with the potential shown in the same spatial grid ($1000\,\text{nm}\times 420\,\text{nm}$). Initially, the wavepacket moves rightward with time as a free wave. At time around $t=30$ fs, one starts to observe the distortion in the wave packet caused by its interaction with the potential. At around $t=60$ fs, a significant portion of the wave packet is reflected by the barriers. Further along in time one can also see clearly the formation of trapped wave packet between the two potential barriers and its gradual decay.

Since the wave function $\psi(x,y,t)$ contains complete quantum-mechanical information about the system under study, we can derive from it all possible observables such as reflection and transmission coefficients, lifetime of the trapped states, phase shifts. The energy spectrum (or the density of states) can also be obtained from the time propagation of system wave functions by using the time-energy Fourier transform. In this way, one can filter out intensity weighted spectra from the correlation function defined as the overlap integral of $\psi(x,y,t)$ with $\psi(x,y,t=0)$.[46,47]

As another illustration of the time evolution of the system we show, in Fig. 4, its wave function in momentum space. At time $t=0$, the momentum contribution is a Gaussian centered at $p_x=0.07$ a.u. and $p_y=0$. At time around $t=30$ fs, we start to see a much wider spread in the momentum wave function including negative components. This corresponds to the compression in the spatial wave function shown in Fig. 3 ($t=30$ fs). At $t=60$ fs a significant part of the wave function has negative momentum in the x direction due to the increasing reflected flux. At $t=210$ fs, the positive and negative parts of the wave function in momentum space are well separated, representing transmission and reflection respectively. Note that we still have a small part of the wavefunction with near-zero momentum, which represents the trapped states.

The effect of increasing the height of the double barrier is shown in Fig. 5. As expected, complete transmission is observed for sufficiently low barriers. As the height of the barriers approaches the incident energy, part of the wave packet is reflected, part of the wave packet tunnels through the barriers, and the rest is temporarily trapped between the two barriers. The ratio of the three parts and their relative phases depend entirely on the structure of the potential and the initial energy value. For sufficiently high barriers, a complete reflection is achieved.

There is a general deep concern about the accuracy of the final system wave function obtained using time-dependent propagation approaches, since errors accumulated over many time steps (normally in the order of hundreds of thousand time steps) may cause severe distortion of the wave packets. Even for one-step time propagators, such as the Chebyshev scheme, errors may accumulate when using repetitively the recurrence relation Eq. (5). Typical number of iterations range from a few hundred to several thousand. To ensure that the time dependant solution accurately reflects the system being modelled, our calculations were checked against a set of criteria.

First of all, the norm of the wave function must be conserved throughout the time evolution, because the exact time-evolution operator is unitary. Secondly, the energy of the system should also remain constant throughout the time evolution. We found both the norm $\langle\psi(x,y,t)|\psi(x,y,t)\rangle$ and the energy $\langle\psi(x,y,t)|H|\psi(x,y,t)\rangle$ are conserved to 1 part in 10^{13} for all of our calculations. The preservation of norm and energy serve as basic criteria to any propagation schemes. For the Chebyshev scheme these two attributes are particularly important, since the Chebyshev propagator is not unitary and thus neither norm nor energy conserving by definition. In this case, conservation of norm and energy puts forward a stringent test to the propagation scheme and the computer code.

Thirdly, we set the external potential to zero, i.e., the wave packet propagates in free space. In this case, the exact analytical solution is known.[46] The absolute error between the exact analytical solution and our numerical propagation of a Gaussian wave function through free space is shown in Fig. 6(a). It is found that the maximum error is in the order of 10^{-12}.

Lastly, since the Schrödinger equation is symmetric with respect to time reversal, a stringent test of reliability of the

solution is to reverse the evolution with time and the wave function should return to its initial state.[48] If errors were accumulated along the way, a reverse propagation would lead to something quite different from the starting wave function. This test was performed by propagating the initial wave function forward in time for $t=210$ fs under the influence of the double-barrier potential as shown in Fig. 3. The resulting wave function was then propagated backward in time by replacing t with $-t$ in Eq. (3). Our results show that the wave function is gradually packed together and finally, at $t=0$, it looks the same as the initial starting wave function. The absolute error is found to be less than 3×10^{-12} as shown in Fig. 6(b). It was this last test that really convinced us that our calculations are highly reliable.

It takes around 35 min of CPU time to complete one of the calculations presented above on a 500 MHz. Digital Alpha personal workstation. Typical memory requirement is 40 Mb. The code is also optimised for parallel computer architectures. About 95% vectorisation has been achieved on the Fujitsu VPP300 supercomputer due to a highly vectorisable FFT routine in use. The CPU time required to complete a typical calculation on the supercomputer is about 5 min. Greater speed improvement is expected when larger arrays are used for simulating more complex nano quantum waveguides.

IV. CONCLUSION

In conclusion, we have presented a highly accurate and effective theoretical model to study quantum-transport phenomena in nano electronic devices. By solving the time-dependent Schrödinger equation, we have quantum-mechanically complete information on the system under study at all times and we can extract values for any measurable quantities of interest. Stringent tests on the accuracy of our solutions were carried out, including conservation of norm and energy, time reversal propagation, and comparison with exact solutions in the case of free space propagation. This model can be readily applied to other nanometer-scale quantum waveguides with arbitrarily complex boundaries.

ACKNOWLEDGMENTS

J.B.W. would like to thank J. F. Williams, B. Stamps, and J. Pan for helpful discussions. We acknowledge a grant of computer time from the Australian National University Supercomputing Facility for use of its Fugitsu VPP300 Super Computer, on which some of the reported calculations were performed.

[1] S. Saini, Nanotechnology **7**, 224 (1996).
[2] L. Kouwenhoven and C. Marcus, Phys. World **11**, 35 (1998).
[3] L. L. Sohn, Nature **394**, 131 (1998).
[4] S. Datta and M. J. McLennan, Rep. Prog. Phys. **53**, 1003 (1990).
[5] H. Luth, Acta Phys. Pol. A **90**, 667 (1996).
[6] D. Goldhabergordon, H. Shtrikman, D. Mahalu, D. Abuschmagder, U. Meirav, and M. A. Kastner, Nature **391**, 156 (1998).
[7] E. N. Bogachek, A. G. Scherbakov, and U. Landman, Phys. Rev. B **56**, 14 917 (1997).
[8] A. Vanoudenaarden, M. H. Devoret, Y. V. Nazarov, and J. E. Mooij, Nature (London) **391**, 768 (1998).
[9] V. Madhavan *et al.* Science **280**, 567 (1998).
[10] M. J. Kelly, *Low Dimensional Semiconductors: Materials, Physics, Technology, Devices* (Oxford, New York, 1995).
[11] L. Kouwenhoven, Science **275**, 1896 (1997).
[12] J. A. Del Alamo, C. C. Eugster, Q. Hu, M. R. Melloch, and M. J. Rooks, Superlattices Microstruct. **23**, 121 (1998).
[13] S. Frank *et al.*, Science **280**, 1744 (1998).
[14] G. J. Jin, Z. D. Wang, A. Hu, and S. S. Jiang, J. Appl. Phys. **85**, 1597 (1999).
[15] Y. P. Varshini, Superlattices Microstruct. **23**, 145 (1998).
[16] K. Nikolic and R. Sordan, Phys. Rev. B **58**, 9631 (1998).
[17] B. Y. Gu, W. D. Sheng, and J. Wang, Int. J. Mod. Phys. B **12**, 653 (1998).
[18] J. P. Carini, J. T. Londergan, D. P. Murdock, D. Trinkle, and C. S. Yung, Phys. Rev. B **55**, 9842 (1997).
[19] I. J. Clark and A. J. Bracken, J. Phys. A **29**, 4527 (1996).
[20] H. Tachibana and H. Totsuji, J. Appl. Phys. **79**, 7021 (1996).
[21] I. Y. Popov and S. L. Popova, Phys. Lett. A **222**, 286 (1996).
[22] H. R. Frohne, M. J. Mclennan, and S. Datta, J. Appl. Phys. **66**, 2699 (1989).
[23] Y. Wang, J. Wang, and H. Guo, Phys. Rev. B **49**, 1928 (1994).
[24] K. Amemiya and K. Kawamura, J. Phys. Soc. Jpn. **64**, 1245 (1995).
[25] P. A. Knipp and T. L. Reinecke, Phys. Rev. B **54**, 1880 (1996).
[26] K. Amemiya, J. Phys. Soc. Jpn. **68**, 567 (1999).
[27] H. Tal-Ezer and R. Kosloff, J. Chem. Phys. **81**, 3967 (1984).
[28] C. Cerjan and K. C. Kulander, Comput. Phys. Commun. **63**, 529 (1991).
[29] G. J. Kroes and D. Neuhauser, J. Chem. Phys. **105**, 8690 (1996).
[30] N. Balakrishnan, C. Kalyanaraman, and N. Sathyamurthy, Phys. Rep. **280**, 80 (1997).
[31] S. K. Gray and G. G. Balintkurti, J. Chem. Phys. **108**, 950 (1998).
[32] M. A. Kastner , Phys. Today **46** (1), 24 (1993).
[33] B. E. Kane, G. R. Facer, A. S. Dzurak, N. E. Lumpkin, R. G. Clark, L. N. Pfeiffer, and K. W. West, Appl. Phys. Lett. **72**, 3506 (1998).
[34] R. A. Webb, Superlattices Microstruct. **23**, 969 (1998).
[35] L. Jacak, P. Hawrylak, and A. Wojs, *Quantum Dot* (Springer-Verlag, Berlin, 1998).
[36] B. K. Tanner, *Introduction to the Physics of Electrons in Solids* (Cambridge University Press, Cambridge, 1995).
[37] C. Kittel, *Introduction to Solid State Physics* (Wiley, New York, 1986).
[38] M. L. Goldberger and K. M. Watson, *Collision Theory* (Wiley, New York, 1964).
[39] J. R. Taylor, *Scattering Theory: Quantum Theory of Nonrelativistic Collisions* (Wiley, New York, 1972).
[40] E. A. McCullough and R. E. Wyatt, J. Chem. Phys. **54**, 3578 (1971).
[41] A. Asker and A. S. Cakmak, J. Chem. Phys. **68**, 2794 (1978).
[42] M. S. Pindzola and D. R. Schultz, Phys. Rev. A **53**, 1525 (1996).

[43] M. D. Feit, J. A. Fleck, and A. Steiger, J. Comput. Phys. **47**, 412 (1982).
[44] M. Braun, C. Meier, and V. Engel, Comput. Phys. Commun. **93**, 152 (1996).
[45] J. B. Wang and T. T. Scholz, Phys. Rev. A **57**, 3554 (1998).
[46] J. M. Feagin, *Quantum Methods with Mathematica* (Springer-Verlag, New York, 1994).
[47] S. Tomsovic and E. J. Heller, Phys. Rev. E **47**, 282 (1993).
[48] V. Mohan and N. Sathyamurthy, Comput. Phys. Rep. **7**, 213 (1988).